Article

Kalman Filter with Adaptive Covariance Estimation for Carrier Tracking under Weak Signals and Dynamic Conditions

Yan Cheng, Shengkang Zhang *, Xueyun Wang, Haifeng Wang and Huijun Yang

Science and Technology on Metrology and Calibration Laboratory, Beijing Institute of Radio Metrology and Measurement, Beijing 100854, China; chengyan178@163.com (Y.C.)
* Correspondence: zhangsk@126.com

Abstract: Kalman filtering (KF)-based tracking has been commonly employed in global navigation satellite system (GNSS) receivers to achieve robust tracking. However, under more serious conditions, such as severe strength attenuation and abrupt dynamic coexisting environments, it is difficult for KF-based tracking to keep tracking well due to the fixed noise statistics. To further enhance the carrier tracking performance, this paper proposes an adaptive KF carrier tracking method for resisting signal strength fading and high dynamic environments. The proposed method introduces the adaptive factor to adjust the process noise covariance to accommodate the noise statistics in actual variable situations. Moreover, we apply the chi-square hypothesis test to detect system stability. The adaptive factor is only applied when the system is not stable, which can enhance computational efficiency. The proposed method is conducted in the GPS L1 software receivers. According to the results, the proposed algorithm can improve the robustness in tracking performance compared with other tracking methods under signal serious fading and high dynamic conditions. Using the proposed method, GNSS receivers' navigation performance can be improved under complex conditions.

Keywords: GNSS receivers; tracking loop; adaptive Kalman filter; weak and high dynamic signals; robust carrier tracking

1. Introduction

Global navigation satellite system (GNSS) receivers have been employed in many areas, such as autonomous navigation, transport monitoring, and so on [1]. Now, the positioning accuracy of some GNSS receivers can reach the centimeter level [2]. To achieve high accuracy, the signal acquisition and tracking modules are significant parts of GNSS receivers. The carrier tracking module is used for achieving carrier synchronization between the input navigation signal and the local carrier signal, which can eliminate the carrier from the navigation signal. The carrier tracking loop usually uses the PLL (phase-locked loop) and the FLL (frequency-locked loop). However, these loops cannot work very well under signal degraded and high dynamic conditions, such as dense foliage, or city overpasses, which frequently appear in complex environments. The PLL has a dilemma between the coherent integration time and the loop bandwidth, which makes it easy to lose lock in weak and high dynamic conditions [3]. The FLL's measurement accuracy is worse than that of the PLL. Accordingly, the traditional tracking loop does not work well under harsh environments.

To address these problems, the KF (Kalman filter) is implemented in the carrier tracking loop because of its robustness in tracking performance [4]. The KF technique has been employed in many areas, such as navigation [5,6], satellite attitude estimation [7,8], unmanned aerial vehicles [9], high accuracy positioning [10], and so on. Psiaki and Jung [11] designed a KF-based tracking loop that can enhance the tracking sensitivity compared with PLL. Won et al. [12] analyzed the characteristics of the KF-based tracking method. Won et al. [13] and Salem et al. [14] both illustrated that the KF-based tracking loop shows better

tracking sensitivity and can obtain more accurate state estimations than the conventional tracking loop under weak signal conditions. Nevertheless, the KF estimation performance is determined by accurate dynamic and stochastic models. The process noise covariance matrix ($\mathbf{Q}_k$) can influence Kalman gains during the whole filtering process. If there are errors in the noise covariances, the filtering estimations may be suboptimal or even divergent.

However, accurate noise covariances are usually difficult to determine due to complex environments. Moreover, in variable situations, the actual noise covariances are changeable and cannot be obtained precisely. In fact, the noise covariance matrices in KF are predefined before the filtering process, which will not be changed anymore in the system. The predetermined noise covariances are typically obtained from the empirical analysis, which is not suitable for the actual noise stochastic properties under time-varying environments [15]. To enhance the KF performance's robustness, many adaptive Kalman filter (AKF) algorithms have been proposed. Liu et al. [16] and Farina et al. [17] have employed different AKF algorithms in integrated navigation systems and localization systems to improve estimation performance. Apart from linear KF systems, non-linear functions also need to adjust the covariance matrices to improve the filtering adaptivity [18,19].

In addition, there are also several AKF algorithms applied in the carrier tracking system. Yao et al. [20] proposed a novel adaptive two-stage KF for tracking loops in high dynamic conditions. Chen et al. [21] proposed a novel adaptive joint Kalman filter algorithm for the vector PLL, but this is not suitable for the scalar tracking loop. Harsha et al. [22] and Vila et al. [23] proposed the adaptive EKF (extended Kalman filter) method for carrier tracking, which is only fit for ionospheric scintillation conditions. Miao et al. [24] proposed the variational Bayesian adaptive cubature Kalman filter algorithm for high dynamic signal conditions. However, there is not enough research on weak and high dynamic signal conditions. In signal fading and high dynamic environments, the signal strength and the Doppler frequency are both variable and sometimes change rapidly. The KF carrier tracking with unchanged noise covariance matrices cannot obtain optimal estimations in this situation, or they even lose lock. Therefore, it is necessary to apply an appropriate AKF algorithm to enhance the carrier tracking's performance under weak signals and high dynamic conditions.

In this research, we propose an AKF carrier tracking approach for weak signals and high dynamic conditions. The adaptive factors are analyzed and designed to adjust the process noise covariance matrix $\mathbf{Q}_k$ adaptively, which can compensate for modeling errors due to the inaccurate $\mathbf{Q}_k$ matrix. Moreover, this algorithm introduces the chi-square method to detect the system's stability. The adaptive factor is used only when the system is not steady. Based on the GPS L1 software receiver experiment results, the proposed AKF tracking shows higher robustness of tracking performance under signal fading and high dynamic conditions.

The other sections are structured as follows. Section 2 illustrates the model of KF-based carrier tracking. Section 3 introduces the proposed AKF carrier tracking loop. Then, the experiment results and analyses are demonstrated in Section 4 and the proposed AKF tracking's performance is validated. Finally, Section 5 draws conclusions.

2. KF-Based Tracking Algorithm

2.1. The Receiver Tracking Loop Model

The KF-based tracking loop's block diagram is presented in Figure 1. Firstly, the digital IF (intermediate frequency) signal is separated into in-phase and the quadrature channels, which are multiplied separately by the sin and cos local replica carrier signals. These results are multiplied by the prompt local replica code. Then, we can obtain the correlated signals. The carrier NCO (numerically controlled oscillator) is applied to produce the local replica carrier signal.
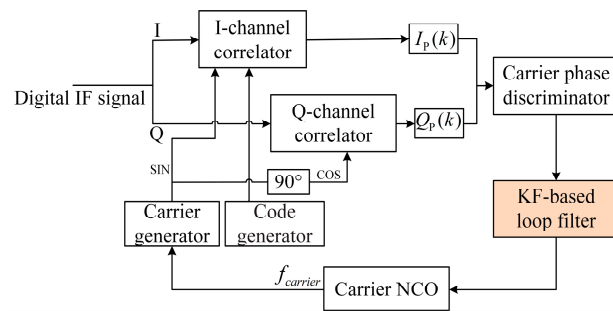
Figure 1. Block diagram of the KF-based carrier tracking loop. (I denotes in-phase, Q denotes quadrature).

After the correlator, the coherent integration values $I_p(k)$ and $Q_p(k)$ can be obtained. $I_p(k)$ and $Q_p(k)$ are input into the discriminator to generate carrier phase error, that is the KF-based loop filter's measurement values. Finally, the carrier phase and frequency of the carrier NCO are updated by the KF loop filter's estimated results. The ultimate aim is to ensure that the local carriers can remain consistent with the received carrier signals, and then the received IF signals' carrier can be completely wiped off.

2.2. System Model

For the KF tracking loop, the state space model can be given by the following:

$$\mathbf{x}_k = \mathbf{\Phi}\mathbf{x}_{k-1} + \mathbf{n}_{k-1} \tag{1}$$

$$\mathbf{z}_k = \mathbf{H}\mathbf{x}_k + v_k \tag{2}$$

where $\mathbf{x}_k = \begin{bmatrix} \Delta\varphi_k & \omega_k & \alpha_k \end{bmatrix}^T$, $\mathbf{\Phi} = \begin{bmatrix} 1 & T & T^2/2 \\ 0 & 1 & T \\ 0 & 0 & 1 \end{bmatrix}$, $\mathbf{z}_k = \delta\varphi_k$, and $\mathbf{H} = \begin{bmatrix} 1 & T/2 & T^2/6 \end{bmatrix}$.

$\Delta\varphi_k$, ω_k, and α_k are, respectively, the carrier phase error, carrier Doppler error, and carrier Doppler frequency rate error. T denotes the tracking loop's update period. $\delta\varphi_k$ denotes the measurement value obtained from the phase discriminator.

In (1), $\mathbf{n}_k$ denotes the system noise, and the corresponding covariance matrix $\mathbf{Q}_k$ is [25]

$$\mathbf{Q}_k = \left(\frac{\omega_{rf}}{C}\right)^2 q_a \begin{bmatrix} T^5/20 & T^4/8 & T^3/6 \\ T^4/8 & T^3/3 & T^2/2 \\ T^3/6 & T^2/2 & T \end{bmatrix}$$
$$+\omega_{rf}^2 q_d \begin{bmatrix} T^3/3 & T^2/2 & 0 \\ T^2/2 & T & 0 \\ 0 & 0 & 0 \end{bmatrix} + \omega_{rf}^2 q_b \begin{bmatrix} T & 0 & 0 \\ 0 & 0 & 0 \\ 0 & 0 & 0 \end{bmatrix} \tag{3}$$

where q_d and q_b are, respectively, the power spectral density of the local oscillator frequency noise and phase noise. q_a represents the power spectral density of the receiver-satellite line-of-light acceleration disturbance. C is the light velocity. ω_{rf} is the nominal carrier frequency.

The measurement noise in Equation (2) is v_k. The covariance matrix $\mathbf{R}_k$ of v_k is obtained as follows [3]:

$$\mathbf{R}_k = \mathrm{E}\left[v_k v_k^T\right] = \frac{1}{2T(c/n_0)_k}\left(1 + \frac{1}{2T(c/n_0)_k}\right) \tag{4}$$

where $(c/n_0)_k$ represents the signal carrier-to-noise ratio.

According to the system model in (1) and (2), the KF algorithm is summarized as follows:

$$\hat{\mathbf{x}}_k^- = \mathbf{\Phi}\hat{\mathbf{x}}_{k-1} \tag{5}$$

$$\hat{\mathbf{P}}_k^- = \mathbf{\Phi}\hat{\mathbf{P}}_{k-1}\mathbf{\Phi}^T + \mathbf{Q}_{k-1} \tag{6}$$

$$\mathbf{K}_k = \hat{\mathbf{P}}_k^- \mathbf{H}^{\mathrm{T}} \left(\mathbf{H} \hat{\mathbf{P}}_k^- \mathbf{H}^{\mathrm{T}} + \mathbf{R}_k \right)^{-1} \tag{7}$$

$$\hat{\mathbf{x}}_k = \hat{\mathbf{x}}_k^- + \mathbf{K}_k \left(\mathbf{z}_k - \mathbf{H}\hat{\mathbf{x}}_k^- \right) \tag{8}$$

$$\hat{\mathbf{P}}_k = (\mathbf{I} - \mathbf{K}_k \mathbf{H}) \hat{\mathbf{P}}_k^- \tag{9}$$

where $\mathbf{K}_k$ denotes the Kalman gain, which can update the weight between measurement values and predicted values of the system model. $\hat{\mathbf{x}}_k^-$ and $\hat{\mathbf{P}}_k^-$ denote the predicted estimation and covariance matrix of the state vector. $\hat{\mathbf{x}}_k$ and $\hat{\mathbf{P}}_k$ denote the estimated values and covariance matrix.

3. Proposed Adaptive KF-Based Tracking

Inadequate prior knowledge of process noise statistics would lead to suboptimal KF estimations or divergence. In the GNSS signal fading and high dynamic applications, the actual noise statistics are not fixed but variable. Accordingly, the noise statistics determined beforehand in the KF tracking are not sufficient to satisfy the practical situations. To enhance the KF tracking performance, an adaptive approach is proposed to tune the process noise covariance $\mathbf{Q}_k$ to satisfy the variable environments.

3.1. Analysis of the Adaptive Factor

The innovation sequence can be used as a reliable indicator of the estimation performance, which is defined as the discrepancy between the actual measurement and the predicted result, as given below:

$$\mathbf{d}_k = z_k - \mathbf{H}\hat{\mathbf{x}}_k^- \tag{10}$$

Then, the innovation covariance is

$$\mathbf{C}_k = \mathrm{E}[\mathbf{d}_k \mathbf{d}_k^T] \tag{11}$$

where $\mathbf{C}_k$ is the actual innovation covariance. In practice, it is difficult to achieve the actual innovation covariance $\mathbf{C}_k = \mathrm{E}[\mathbf{d}_k \mathbf{d}_k^T]$, which can be estimated by the present and past sequences. The window function method is commonly applied for innovation covariance estimation, that is

$$\hat{\mathbf{C}}_k = \frac{1}{N} \sum_{\mathrm{i}=k-N+1}^{k} \mathbf{d}_i \mathbf{d}_i^{\mathrm{T}} \tag{12}$$

where N represents the window length and $\hat{\mathbf{C}}_k$ represents the estimated innovation covariance matrix.

When there are no modeling errors, the innovation sequences follow the orthogonal principle [26], that is

$$\mathrm{E}[\mathbf{d}_{k+j}\mathbf{d}_k^{\mathrm{T}}] = 0, \ k=1,2\cdots, \ j=1,2\cdots \tag{13}$$

However, when modeling errors exist in the filtering system, the orthogonal principle cannot follow well. Therefore, the proposed adaptive tuning method should make the system obey the orthogonal principle. The orthogonal principle can make useful information of the innovation sequences completely extracted.

Because the fixed $\mathbf{Q}_k$ matrix of KF may be inconsistent with the variable practical situation, the adaptive factor is used to adjust the matrix $\mathbf{Q}_k$. Accordingly, the predicted state error covariance matrix $\hat{\mathbf{P}}_k^-$ is given as

$$\hat{\mathbf{P}}_k^- = \mathbf{\Phi}\hat{\mathbf{P}}_{k-1}\mathbf{\Phi}^{\mathrm{T}} + \lambda_k \mathbf{Q}_{k-1} \tag{14}$$

where λ_k is the adaptive factor, which should be computed according to (13) so that the innovation sequences can follow the orthogonal principle.

If the KF state estimations are quite accurate, the state estimate error $\tilde{\mathbf{x}}_k = \mathbf{x}_k - \hat{\mathbf{x}}_k$ could follow $\mathrm{O}\left[\left|\tilde{\mathbf{x}}_k\right|^2\right] \ll \mathrm{O}\left[\left|\tilde{\mathbf{x}}_k\right|\right]$. Then the following can be obtained [27]:

$$\mathrm{E}[\mathbf{d}_{k+j}\mathbf{d}_k^{\mathrm{T}}] \approx \mathbf{H}\boldsymbol{\Phi}(\mathbf{I} - \mathbf{K}_{k+j-1}\mathbf{H}_{k+j-1}) \bullet \cdots \bullet \boldsymbol{\Phi}(\mathbf{I} - \mathbf{K}_{k+2}\mathbf{H}_{k+2}) \bullet \\ \boldsymbol{\Phi}(\mathbf{I} - \mathbf{K}_{k+1}\mathbf{H}_{k+1})\boldsymbol{\Phi}(\hat{\mathbf{P}}_k^-\mathbf{H}^{\mathrm{T}} - \mathbf{K}_k\mathbf{C}_k) \quad j = 1, 2 \cdots \tag{15}$$

where $\mathbf{I}$ denotes the identity matrix. Therefore, if the time-varying gain matrix $\mathbf{K}_k$ is chosen appropriately for all $j = 1, 2, \ldots$ to make

$$\hat{\mathbf{P}}_k^-\mathbf{H}^{\mathrm{T}} - \mathbf{K}_k\mathbf{C}_k = 0 \tag{16}$$

then the orthogonal principle $\mathrm{E}[\mathbf{d}_{k+j}\mathbf{d}_k^{\mathrm{T}}] = 0$ can be satisfied.

Substituting (7) into (16), we have

$$\hat{\mathbf{P}}_k^-\mathbf{H}^{\mathrm{T}}\left\{\mathbf{I} - \left(\mathbf{H}\hat{\mathbf{P}}_k^-\mathbf{H}^{\mathrm{T}} + \mathbf{R}_k\right)^{-1}\mathbf{C}_k\right\} = 0 \tag{17}$$

The sufficient condition for Equation (17) is as follows:

$$\left(\mathbf{H}\hat{\mathbf{P}}_k^-\mathbf{H}^{\mathrm{T}} + \mathbf{R}_k\right)^{-1}\bullet\mathbf{C}_k = \mathbf{I} \tag{18}$$

Therefore,

$$\mathbf{H}\hat{\mathbf{P}}_k^-\mathbf{H}^{\mathrm{T}} + \mathbf{R}_k = \mathbf{C}_k \tag{19}$$

Substituting (14) into (19), it can be obtained that

$$\mathbf{C}_k = \mathbf{H}\boldsymbol{\Phi}\hat{\mathbf{P}}_{k-1}\boldsymbol{\Phi}^{\mathrm{T}}\mathbf{H}^{\mathrm{T}} + \mathbf{R}_k + \lambda_k\mathbf{H}\mathbf{Q}_{k-1}\mathbf{H}^{\mathrm{T}} \tag{20}$$

Define

$$\mathbf{A}_k \triangleq \mathbf{H}\boldsymbol{\Phi}\hat{\mathbf{P}}_{k-1}\boldsymbol{\Phi}^{\mathrm{T}}\mathbf{H}^{\mathrm{T}} + \mathbf{R}_k \tag{21}$$

$$\mathbf{B}_k \triangleq \mathbf{H}\mathbf{Q}_{k-1}\mathbf{H}^{\mathrm{T}} \tag{22}$$

Then (20) can be rewritten as

$$\mathbf{C}_k - \mathbf{A}_k = \lambda_k\mathbf{B}_k \tag{23}$$

The trace of (23) is as follows:

$$\mathrm{tr}(\mathbf{C}_k - \mathbf{A}_k) = \mathrm{tr}(\lambda_k\mathbf{B}_k) \tag{24}$$

where tr() represents the trace of the matrix. Then, λ_k is obtained:

$$\lambda_k = \frac{\mathrm{tr}(\mathbf{C}_k - \mathbf{A}_k)}{\mathrm{tr}(\mathbf{B}_k)} \tag{25}$$

The actual innovation covariance $\mathbf{C}_k$ is difficult to obtain, which is typically estimated by $\hat{\mathbf{C}}_k$ in (12). To decrease the computational burden, the recursive algorithm is applied in (12) to estimate the innovation covariance [28]:

$$\hat{\mathbf{C}}_k = \hat{\mathbf{C}}_{k-1} + \frac{1}{N}\left(\mathbf{d}_k\mathbf{d}_k^T - \mathbf{d}_{k-N}\mathbf{d}_{k-N}^T\right) \tag{26}$$

where N is the window length of the sliding window, which should be correctly determined. Because if the window length is too small, it is difficult to obtain an unbiased estimate. On the contrary, if the window size is too large, the estimations cannot reflect the short-term statistics of innovation covariances. Jwo et al. [29] stated that a good window size is between 10 and 30.

Then, the adaptive factor λ_k can be obtained as follows:

$$\lambda_k = \frac{\mathrm{tr}(\hat{\mathbf{C}}_k - \mathbf{A}_k)}{\mathrm{tr}(\mathbf{B}_k)} \tag{27}$$

In dynamic and weak signal conditions, tracking systems often involve high levels of uncertainty in the system model. The larger adaptive factor can reduce its reliance on the system model and place more trust in the measurements, which can effectively remove the impact of model uncertainty. Accordingly, to keep the state estimation accuracy, the adaptive factor should not be smaller than 1.

If the adaptive factor is larger than 1, indicating that the tracking system changes suddenly, the value of $\hat{\mathbf{P}}_k^-$ will increase based on Equation (14). Meanwhile, the Kalman gain $\mathbf{K}_k$ will increase according to Equation (7). Accordingly, based on Equation (8), more weight will be put on the measurement data, and then the accuracy of the state estimation will be improved [30]. A larger adaptive factor can respond more quickly to changes in the measurements. This can accelerate the convergence rate of the filter and provide more timely estimation results, adapting to the variations of the signal. Hence, the robustness and accuracy of the system can be improved. Then, the adaptive factor λ_k should be as follows:

$$\lambda_k = \max\left\{1, \ \frac{\mathrm{tr}(\hat{\mathbf{C}}_k - \mathbf{A}_k)}{\mathrm{tr}(\mathbf{B}_k)}\right\} \ k = 1, 2 \cdots \tag{28}$$

3.2. The System Stability Detection

If the system remains stable, there is no need to employ the adaptive factor in the KF process. Excessive use of adaptive factors may reduce the filtering accuracy and increase the computational load. The adaptive factor is used only when the system is not steady. Hence, the hypothesis testing method is employed to test the system. Then, two hypotheses can be introduced:

γ_0: the system operates in a stable state;

γ_1: the system operates abnormally.

When the tracking system is stable, the innovation sequence $\mathbf{d}_k$ follows Gaussian distribution with a zero mean [26]. Otherwise, when the tracking system is not stable, $\mathbf{d}_k$ will not obey the Gaussian distribution. Therefore, the detailed expressions are as follows:

If the system is stable, then $\mathbf{d}_k \sim \mathrm{N}\big(0, \hat{\mathbf{C}}_k\big)$;

If the system is not stable, then $\mathbf{d}_k$ does not obey the Gaussian distribution.

Therefore, the system stability detection is realized by these characteristics.

According to the chi-square test, based on $\mathbf{d}_k$, the statistics function is defined as follows:

$$\beta_k = \mathbf{d}_k^{\mathrm{T}} \hat{\mathbf{C}}_k^{-1} \mathbf{d}_k \tag{29}$$

If $\mathbf{d}_k$ obeys a Gaussian white noise sequence, β_k has χ^2 distribution with s-degree-of-freedom (s-DOF) and s denotes the innovation sequence's dimension.

If α is chosen as the significance level, then

$$\mathrm{P}\left\{x > \chi_\alpha^2(s)\right\} = \int_{\chi_\alpha^2(n)}^{\infty} f(x)dx = \alpha, \ 0 < \alpha \leq 1 \tag{30}$$

where x is the statistic of the χ^2 distribution. $\chi_\alpha^2(s)$ is the threshold value which is decided by the given α and s [31]. Figure 2 shows the PDF (probability density function) of the chi-square distribution.

Accordingly, if the hypothesis γ_1 is established, β_k will be greater than $\chi_\alpha^2(s)$, which indicates that the system is not stable. Otherwise, the system is in a stable state.
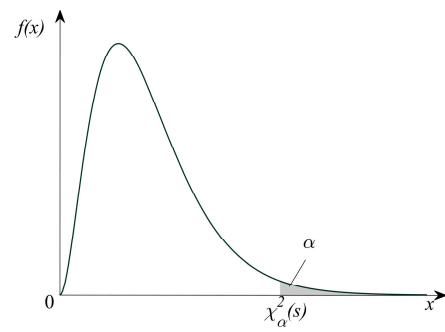
Figure 2. The PDF of the chi-square distribution.

3.3. The Proposed Algorithm for Carrier Tracking

In the carrier tracking loop, $\mathbf{z}_k$ is a scalar in the epoch k, then $\mathbf{d}_k$ and $\boldsymbol{\beta}_k$ are both scalars. Hence, the β_k has the χ^2 distribution with 1-DOF:

$$\beta_k \sim \chi^2(1) \tag{31}$$

Figure 3 shows the proposed AKF algorithm. The functions of the two orange blocks are to detect the system stability and adjust the process noise covariance $\mathbf{Q}_k$, respectively. Apart from these two blocks, other parts in Figure 3 mainly follow the standard KF algorithm. Accordingly, the proposed tracking loop architecture is based on Figure 1, while the KF-based loop filter module is replaced by the proposed AKF algorithm. In the proposed algorithm, the measurement noise covariance matrix $\mathbf{R}_k$ remains constant during the filtering process. Reference [32] stated that the $\mathbf{Q}_k$-only adaptive algorithm is superior to the $\mathbf{R}_k$-only and both $\mathbf{Q}_k$ and $\mathbf{R}_k$ adaptive cases in practical estimating performance.
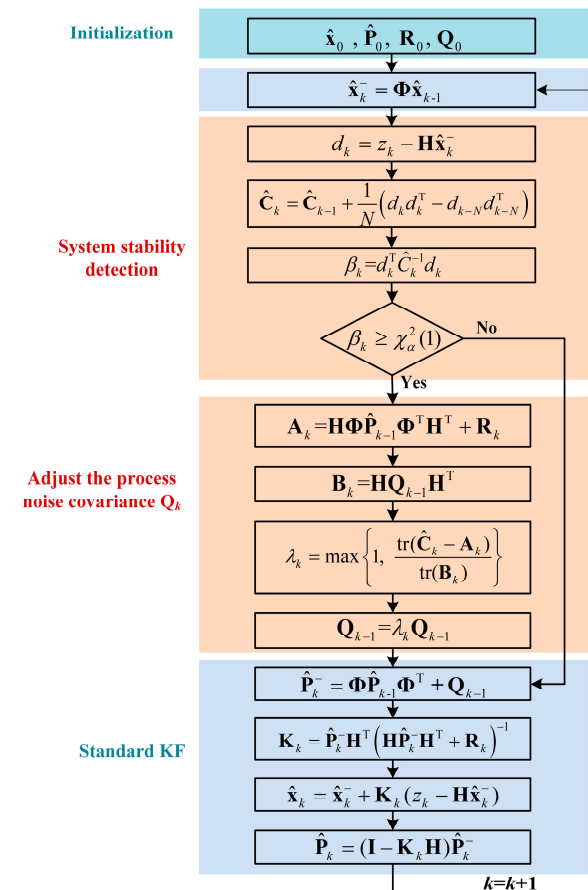

Figure 3. The proposed AKF algorithm's flow chart.

4. Performance Evaluation and Discussion

To assess the validity and superiority of the proposed approach, the software GPS (Global Positioning System) L1 receiver is conducted. The input signal of the software receiver is the IF signal, which is generated by a satellite navigation signal simulator. The frequency and sampling rate of the IF signal are 1.42 MHz and 10 MHz, respectively. The signal resolution is set to 4-bit. Nine channels have been simulated in the software receiver for the visible satellites.

To evaluate the performance, four tracking methods are used in the experiments.
Method 1: the proposed AKF-based tracking method;
Method 2: the conventional PLL tracking method (the PLL's bandwidth is 15 Hz and the update period is 4 ms);
Method 3: the standard KF tracking;
Method 4: the STKF (strong tracking Kalman filter) tracking method.

4.1. Example 1: Signal Fading Rapidly and Acceleration Scenario

Figure 4 demonstrates the simulated fading signal with dynamics. In Figure 4a, the C/N_0 began with 45 dB-Hz for 20 s. Then the C/N_0 was descended by 1 dB per 5 s until it decreased to 25 dB-Hz. Then the signal kept the 25 dB-Hz for 60 s. After 180 s, the C/N_0 was increased by 1 dB per 5 s until reaching the initial signal power. In Figure 4b, during the first 20 s, the receiver halted. After 20 s, the receiver accelerated with 32 m/s^2 and the velocity reached 3200 m/s at t = 120 s. After 120 s, the receiver remained at 3200 m/s until t = 180 s. Then, the receiver decelerated with -32 m/s^2 for 100 s and then stopped at 280 s. The velocity set in the scenario often occurs in aircraft, which is a high dynamic scenario.
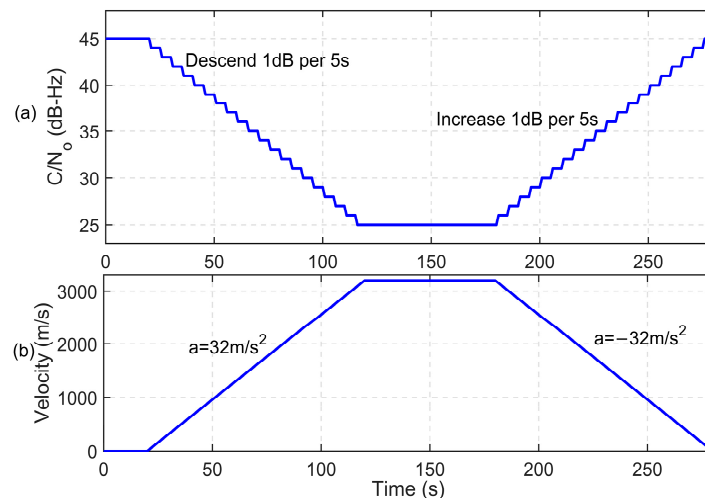

Figure 4. The signal C/N_0 and the velocity of the signals for Example 1: (**a**) the C/N_0 variations of the signals; (**b**) the velocity variations of the signals.

In four tracking methods, the parameters settings are as follows:
Method 1:
The initial parameter settings are listed in Table 1.

Table 1. The initial parameters settings for Method 1.

Parameters	Description	Values
$\mathbf{Q}_k$	Process noise covariance matrix	Using Equation (3) with q_a = 0.3 $(\text{m}^2/\text{s}^6)/\text{Hz}$
$\mathbf{R}_k$	Measurement noise covariance matrix	Using Equation (4) with $(C/N_0)_0$ = 45 dB-Hz
T	Update period of the tracking loop	4 ms
N	Window size for estimated innovation covariances	20
$\chi_\alpha^2(1)$	Threshold value to detect system stability	6.6349

(i) Initialize the process noise covariance matrix $\mathbf{Q}_k$ using (3) with $q_a= 0.3 \; (\mathrm{m^2/s^6})/\mathrm{Hz}$. Initialize the measurement noise covariance $\mathbf{R}_k$ using (4) with $(C/N_0)_0 = 45$ dB-Hz and $(c/n_0)_0 = 10^{4.5}$. The update period of the tracking loop is 4 ms. For the weak and dynamic signals, the update period is a compromise parameter, which should be long enough to work under weak signal conditions and should be as short as possible to work under dynamic conditions simultaneously. Then we set the update period as 4 ms.

(ii) In the proposed method, the window size for estimated innovation covariances is 20. To make a compromise between the unbiased estimation and the short-term statistics, reference [29] has stated that good window size is between 10 and 30.

(iii) Set the significance level α to 0.01, and the threshold value $\chi^2_{0.01}(1)$ is 6.6349. It means that the probability of $\{\beta_k \geq 6.6349\}$ is 0.01. If the event $\{\beta_k \geq 6.6349\}$ occurs, the hypothesis γ_1 will hold and the proposed AKF tracking will be implemented.

Method 2: in the PLL tracking method, the PLL's bandwidth is 15 Hz. The update period of the tracking loop is the same as that in Method 1.

Method 3: in the standard KF tracking, the settings of $\mathbf{Q}_k$, $\mathbf{R}_k$, and loop update interval are the same as those in Method 1.

Method 4: in STKF tracking, the settings of $\mathbf{Q}_k$, $\mathbf{R}_k$, and loop update interval are the same as those in Method 1.

The C/N_0 and Doppler estimated results of the four algorithms for PRN 14 and PRN 19 are shown in Figure 5. Figure 5a,c are the estimated results for PRN 14. Meanwhile, Figure 5b,d are the estimated results for PRN 19. Figure 5 demonstrates that the proposed AKF tracking approach performs best, which can follow the variable signal strength. Other tracking methods cannot follow the weak and dynamic power and deviate from the actual value when the signal is weak. In Figure 5c,d, the Doppler rates for PRN 14 and PRN 19 are 39 Hz/s and 50 Hz/s from 20 s to 120 s, respectively. From 121 s to 180 s, the Doppler rates for PRN 14 and PRN 19 are 3 Hz/s and 23 Hz/s, respectively. The KF tracking and the PLL tracking cannot follow the sudden changes caused by the Doppler frequency variation and signal strength attenuation. KF tracking fails because it cannot update the $\mathbf{Q}_k$ matrix by the adaptive algorithm. The PLL tracking fails because the tracking loop's bandwidth is fixed and cannot adapt to the dynamic and weak signal. For the STKF tracking, although it introduces the fading factors, without the system stability detection and adaptive $\mathbf{Q}_k$, false fading factors can be obtained in the STKF, which leads to wrong estimations. Then, the STKF performance performs worse than the KF. Hence, STKF is difficult to ensure accurate fading factors for all situations [33]. Accordingly, the STKF tracking for PRN 14 is better than KF tracking, but the STKF for PRN 19 is worse than KF. With the system stability detection and $\mathbf{Q}_k$ adaptation, the proposed AKF tracking method can keep tracking well during the whole process.

Figure 6 shows the adaptive factor of the proposed AKF algorithm. As we can observe, when the signal strength decreases quickly while the velocity is accelerating, the adaptive factor λ_k will be turned to a larger value. However, as the signal strength increases, the system keeps track of the signal well and the adaptive factors need not be used.

This indicates that the adaptive process noise covariances play a significant role in adapting to the signal strength and dynamic variation. According to the results, the proposed AKF approach is effective in resisting sudden changes from the power fading and high dynamic of the navigation signal. The proposed AKF tracking shows higher robustness compared with other tracking algorithms. This superiority can improve the position accuracy of dynamic receivers under signal fading environments.
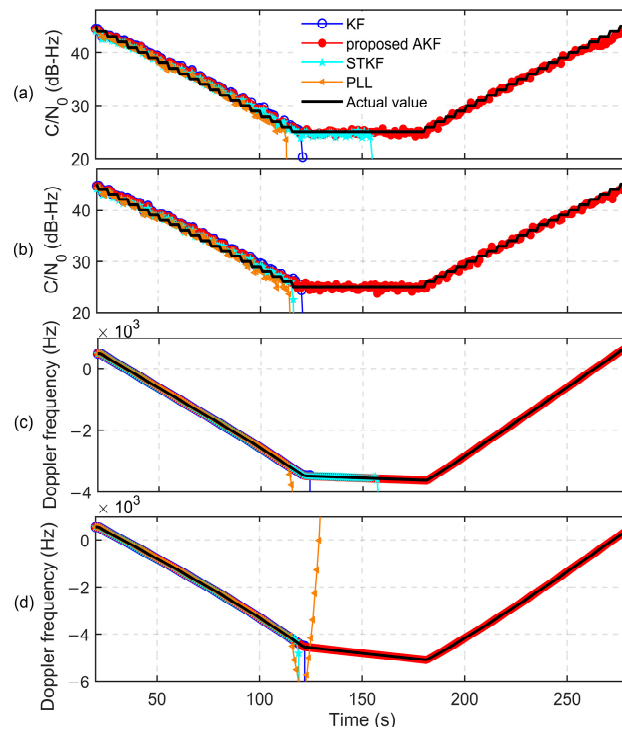
Figure 5. The C/N_0 and Doppler estimated results of the four algorithms for Example 1. (**a**,**c**) are the results for PRN 14 satellite signal; (**b**,**d**) are the results for PRN 19 satellite signal. (PRN: pseudo-random number).
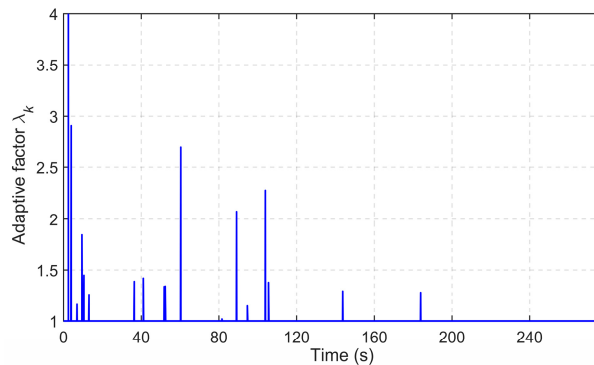

Figure 6. The results of the adaptive factor λ_k in Example 1.

4.2. Example 2: Abrupt Dynamics and Signal Fading Scenario

The second example is used to further verify the proposed algorithm's validity. In Example 1, the dynamics contain acceleration, while Example 2 not only contains acceleration but also contains higher-order dynamics, which are abrupt turns.

This example implements the signal fading and higher-order dynamics simultaneously. Figure 7 demonstrates the signal strength and dynamics for Example 2. For the signal power, the C/N_0 started with 37 dB-Hz, and then was descended by 2 dB per 30 s. The maximum attenuation was 22 dB at 180 s and was kept at 25 dB-Hz for 25 s. The dynamics of the signal are illustrated in Table 2, which has been divided into ten intervals. Figure 7c labels the ten intervals of dynamics to reflect the Doppler variation of PRN 14.
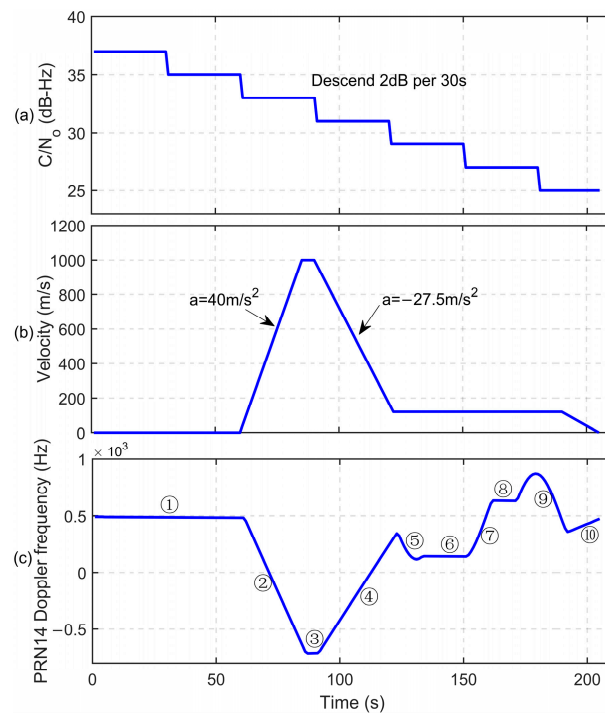
Figure 7. The signal C/N_0, velocity and the Doppler of the signals for Example 2: (**a**) the C/N_0 variation of the signals; (**b**) the velocity variation of the signals; (**c**) the Doppler frequency variation for PRN 14 of the signals (the numbers with circles corresponds to the numbers in Table 2).

Table 2. Description of vehicle motion.

Number	Movement State	Time (s)
1	Stationary	0–60
2	Accelerated (a = 40 m/s^2)	61–85
3	Constant velocity (v = 1000 m/s)	86–90
4	Decelerated (a = −27.5 m/s^2)	91–122
5	1st clockwise turn with 90° (radius r = 763.94 m)	123–132
6	Constant velocity (v = 120 m/s)	133–150
7	2nd clockwise turn with 90° (radius r = 763.94 m)	151–160
8	Constant velocity (v = 120 m/s)	161–170
9	3rd clockwise turn with 180° (radius r = 763.94 m)	171–190
10	Decelerated (a = −8 m/s^2)	191–205

The height of the receiver remains constant during the whole simulation process. Figure 8 shows the trajectory of the receiver. The receiver motion coexisted with acceleration, deceleration, and three abrupt turns. The first two turns turned with 90 degrees and the third one turned with 180 degrees. This scenario is used to simulate the aircraft flying in the sky and passing through obstructions, like forests and so on.

For the parameters set in this test, apart from $\mathbf{R}_k$, the other initial parameters in the four methods are identical to those in Example 1. $\mathbf{R}_k$ is initialized using (4) with C/N_0 = 37 dB-Hz and $(c/n_0)_0 = 10^{3.7}$.

The C/N_0 and Doppler estimated results after 60 s for PRN 14 and PRN 20 are shown in Figure 9. Figure 9a,c show the estimations for PRN 14. Figure 9b,d show the estimations for PRN 20. In Figure 9a,b, all four tracking algorithms can obtain accurate estimated values when the C/N_0 is relatively higher and the receiver motion includes acceleration and abrupt turns. As the C/N_0 decreases below 27 dB-Hz, only the proposed method can follow the signal fading and dynamic signals during the whole process.
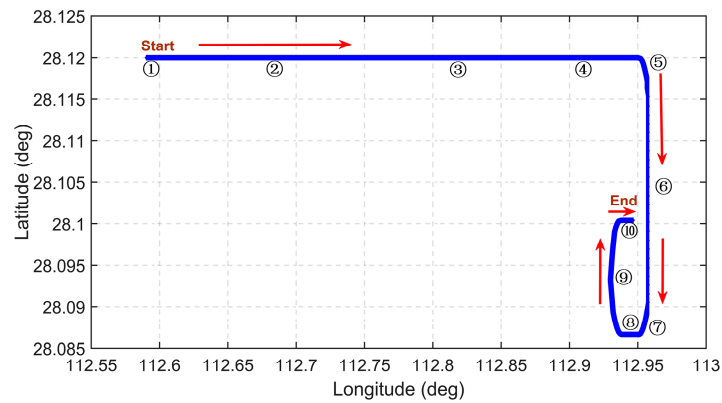
Figure 8. The trajectory of the receiver in the simulation for Example 2. (The numbers with circles corresponds to the numbers in Table 2, and the red arrows denotes the direction of the receiver's movement).
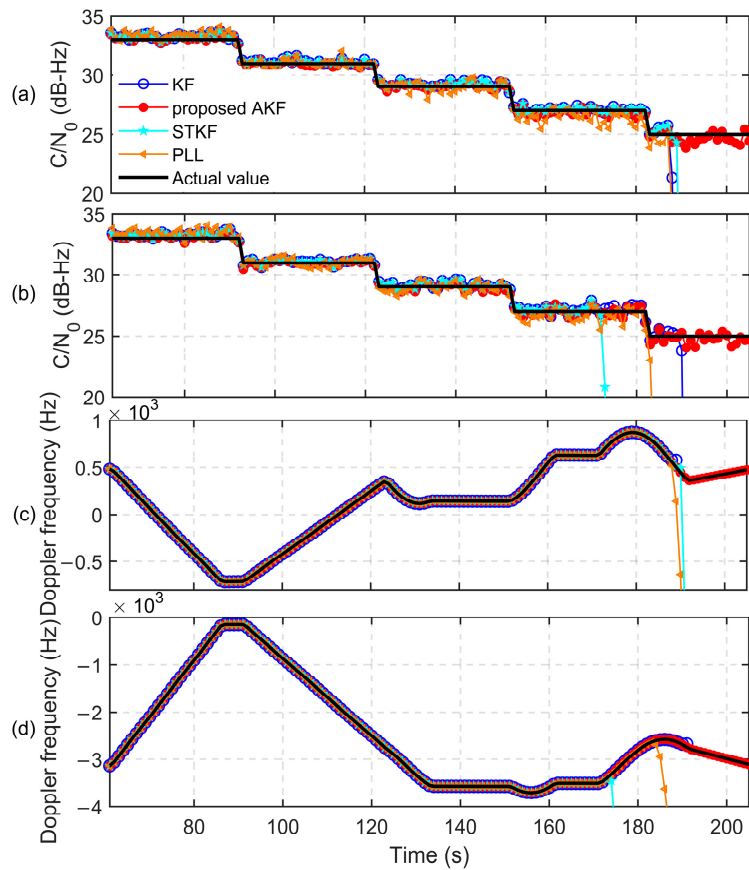

Figure 9. The C/N_0 and Doppler estimated results of the four algorithms after 60 s for Example 2. (**a**,**c**) are the results for the PRN 14 satellite signal; (**b**,**d**) are the results for PRN 20 satellite signal.

When the C/N_0 decreases to 25 dB-Hz and the receiver experiences the third clockwise turn, the PLL method and the KF tracking both cannot work well and lose lock. Because the STKF tracking does not have system stability detection and $\mathbf{Q}_k$ adaptation, the STKF may introduce inaccurate fading factors and perform worse than KF. As shown in Figure 9, the STKF is worse than KF in PRN 20.

The adaptive factor of the proposed AKF algorithms for Example 2 is shown in Figure 10. When the system encounters sudden dynamics, the adaptive factor λ_k will be larger, otherwise, the adaptive factor will be set to 1.
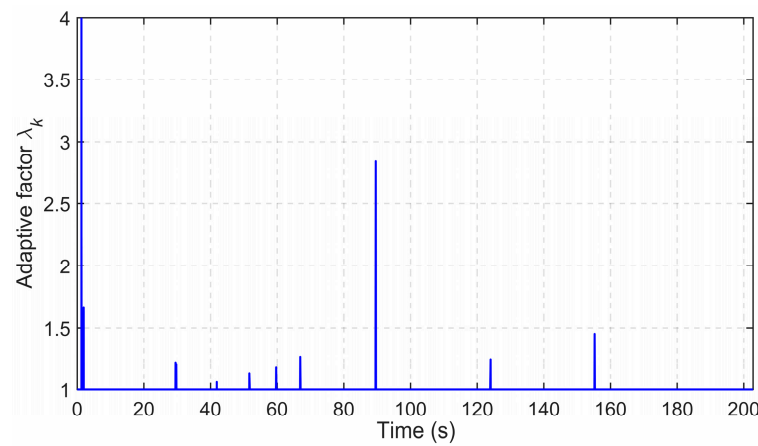
Figure 10. The results of the adaptive factor λ_k in Example 2.

Therefore, for the first two abrupt turns under relatively high C/N_0, all four tracking algorithms can track well. When the third turn is under relatively low C/N_0, the KF and PLL tracking cannot adapt to the signal variation. The serious strength fading and abrupt motion cause the KF and PLL tracking cannot match the actual harsh situations. However, because the proposed adaptive factor can adjust the noise statistics to satisfy the real variable noise environments, the proposed AKF tracking can compensate for the modeling error under harsh environments.

Accordingly, in comparison with other tracking methods, the proposed AKF approach can adapt to the variable signal and show more robust tracking performance when the serious strength fading and sharp turns coincide. The proposed tracking approach can enhance the navigation performance of GPS receivers in complex environments with higher-order dynamic and signal attenuation.

4.3. Complexity Analysis

Compared with the KF-based tracking, the extra computational load in the proposed method is mainly the computation of β_k and λ_k, as shown in Figure 3 marked with the orange blocks. Note that n represents the dimension of the state vector, and m denotes the dimension of the measurement vector. Firstly, the computation of β_k requires three equations shown in Figure 3, and then the computation complexity of β_k is $O(n)$. Three variables d_k, β_k, and $\hat{C}_k$ are scalars, and Table 3 shows the details of three equations for one iteration. For the computation of variable β_k, $d_k{}^2$ has been obtained in the computation of $\hat{C}_k$, so the multiplication number of the variable β_k is 1. Secondly, the calculation of λ_k also needs three equations shown in Figure 3. The computation complexity for $\mathbf{A}_k$ is $O(n^3)$. However, because $\mathbf{\Phi}$ is a 3×3 upper triangular matrix, the computation of $\mathbf{A}_k$ needs 24 multiplications and 14 additions, which is the most time-intensive part. The computation of $\mathbf{B}_k$ needs 12 multiplications and 8 additions. The total operations are 44 multiplications and 28 additions, as demonstrated in Table 3.

Table 3. Computational complexity of β_k and λ_k for one-step iteration.

Function	Variable	Number of Multiplications	Number of Additions
Calculation of β_k	d_k	3	3
	$\hat{C}_k$	3	2
	β_k	1	0
Calculation of λ_k	$\mathbf{A}_k$	24	14
	$\mathbf{B}_k$	12	8
	λ_k	1	1
Total requirements		44	28

According to Lo et al. [34], the multiplication number $M(n, m)$ and the addition number $A(n, m)$ for each KF iteration are as follows:

$$M\left(n, m\right) = 2n^3 + 3n^2m + n^2 + 2nm^2 + 2nm \tag{32}$$

$$A(n, m) = 2n^3 + 3n^2m + 2nm^2 - nm - n \tag{33}$$

For the KF tracking, $n = 3$ and $m = 1$. Hence, $M(n, m)$ and $A(n, m)$ are 102 and 81, respectively.

Accordingly, in comparison with KF tracking, the calculation load of the proposed AKF method increases about 43% of multiplications and 34% of additions. However, the calculation of λ_k is only used when the system works abnormally. When the system operates in the steady state, only β_k needs to be computed, the computational load of which is small, as shown in Table 2. Therefore, in comparison with the KF-based tracking, the extra calculation burden in the proposed AKF method is not heavy.

5. Conclusions

To enhance the tracking robustness in signal attenuation and high dynamic environments, an adaptive KF-based carrier tracking approach is proposed. The proposed approach introduces the adaptive algorithm into the KF algorithm to self-tune the process noise covariance, which makes the tracking approach accommodate the time-varying signals. Moreover, the chi-square method is applied to detect system stability. The AKF algorithm is used when the tracking system is not steady, which can improve accuracy and computational efficiency.

The algorithm has been applied to the GPS L1 software receiver. According to the test results, the proposed carrier tracking algorithm can enhance the tracking robustness in severe fading and high dynamic environments compared with other tracking methods. Accordingly, when the proposed AKF approach is implemented in the GNSS receivers, it can enhance the navigation and positioning accuracy of high-speed receivers moving through obstructions in complicated environments.

For future research, the proposed tracking algorithm can be applied in complex conditions, such as automatic driving or unmanned aerial vehicle navigation systems experiencing high dynamic and signal fading. Moreover, the adaptability of the proposed algorithm can adjust the system noise covariance, which can also be employed in other nonlinear filtering methods, such as unscented KF (UKF), extended KF (EKF), and so on. Our work lays a theoretical foundation for nonlinear filtering and can enhance the filtering robustness in complex conditions. In addition, when the proposed AKF approach is implemented in the GNSS receivers, it can enhance navigation and positioning accuracy in complex environments.

Author Contributions: Conceptualization, Y.C. and S.Z.; methodology, Y.C., X.W. and H.W.; software, Y.C., H.W. and H.Y.; validation, Y.C., S.Z. and X.W.; investigation, Y.C., H.W. and H.Y.; writing—original draft preparation, Y.C.; writing—review and editing, S.Z.; supervision, S.Z.; project administration, X.W. All authors have read and agreed to the published version of the manuscript.

References

1. Yasyukevich, Y.V.; Zhang, B.; Devanaboyina, V.R. Advances in GNSS Positioning and GNSS Remote Sensing. *Sensors* **2024**, *24*, 1200. [CrossRef] [PubMed]
2. Hamza, V.; Stopar, B.; Sterle, O.; Pavlovčič-Prešeren, P. Low-Cost Dual-Frequency GNSS Receivers and Antennas for Surveying in Urban Areas. *Sensors* **2023**, *23*, 2861. [CrossRef] [PubMed]

3. Yang, R.; Ling, V.; Poh, K.; Morton, Y. Generalized GNSS signal carrier tracking: Part II: Optimization and implementation. *IEEE Trans. Aerosp. Electron. Syst.* **2017**, *53*, 1798–1811. [CrossRef]

4. López-Salcedo, J.A.; Del Peral-Rosado, J.A.; Seco-Granados, G. Survey on robust carrier tracking techniques. *IEEE Commun. Surv. Tutor.* **2014**, *16*, 670–688. [CrossRef]

5. Wang, D.; Dong, Y.; Li, Z.; Li, Q.; Wu, J. Constrained MEMS-Based GNSS/INS Tightly Coupled System with Robust Kalman Filter for Accurate Land Vehicular Navigation. *IEEE Trans. Instrum. Meas.* **2020**, *69*, 5138–5148. [CrossRef]

6. Gao, G.; Gao, B.; Gao, S.; Hu, G.; Zhong, Y. A hypothesis test-constrained robust Kalman filter for INS/GNSS integration with abnormal measurement. *IEEE Trans. Veh. Technol.* **2023**, *72*, 1662–1673. [CrossRef]

7. Chen, X.; Cao, L.; Guo, P.; Xiao, B. A higher-order robust correlation Kalman filter for satellite attitude estimation. *ISA Trans.* **2020**, *124*, 326–327. [CrossRef] [PubMed]

8. Wu, M.; He, Y.; Luo, S.; Liu, W. Particle filter-based real-time phase line bias estimation for GNSS-based attitude deter-mination with common-clock receivers. *Adv. Space Res.* **2023**, *71*, 1682–1699. [CrossRef]

9. Liu, Y.; Duan, C.; Liu, L.; Cao, L. Discrete-Time Incremental Backstepping Control with Extended Kalman Filter for UAVs. *Electronics* **2023**, *12*, 3079. [CrossRef]

10. Feng, S.; Ochieng, W.; Moore, T.; Hill, C.; Hide, C. Carrier phase-based integrity monitoring for high-accuracy positioning. *GPS Solut.* **2019**, *13*, 13–22.

11. Psiaki, L.; Jung, H. Extended Kalman filter methods for tracking weak GPS signals. In Proceedings of the 15th International Technical Meeting of the Satellite Division of The Institute of Navigation (ION GPS 2002), Portland, OR, USA, 24–27 September 2002; pp. 2539–2553.

12. Won, J.; Pany, T.; Eissfeller, B. Characteristics of Kalman filters for GNSS signal tracking loop. *IEEE Trans. Aerosp. Electron. Syst.* **2012**, *48*, 3671–3681. [CrossRef]

13. Won, H.; Dotterbock, D.; Eissfeller, B. Performance comparison of different forms of Kalman filter approach for a vector-based GNSS signal tracking loop. *Navigation* **2010**, *57*, 185–199. [CrossRef]

14. Salem, D.; O'Driscoll, C.; Lachapelle, G. Methodology for comparing two carrier phase tracking techniques. *GPS Solut.* **2012**, *16*, 197–207. [CrossRef]

15. Feng, B.; Fu, M.; Ma, H.; Xia, Y.; Wang, B. Kalman filter with recursive covariance estimation-sequentially estimating process noise covariance. *IEEE Trans. Ind. Electron.* **2014**, *61*, 6253–6263. [CrossRef]

16. Liu, Y.; Fan, X.; Lv, C.; Wu, J.; Li, L.; Ding, D. An innovative information fusion method with adaptive Kalman filtering for integrated INS/GPS navigation of autonomous vehicles. *Mech. Syst. Signal Process.* **2018**, *100*, 605–616. [CrossRef]

17. Farina, B.; Tolado, J.; Acosta, L. Augmented Kalman filter design in a localization system using onboard sensors with intrinsic delays. *IEEE Sens. J.* **2023**, *23*, 12105–12113. [CrossRef]

18. Curbelo, E.; Martino, L.; Llorente, F.; Delgado-Gomez, D. Adaptive Posterior Distributions for Uncertainty Analysis of Covariance Matrices in Bayesian Inversion Problems for Multioutput Signals. *viXra* **2023**. viXra:2310.0032.

19. Martino, L.; Llorente, F.; Cuberlo, E.; Lopez-Santiago, J.; Miguez, J. Automatic Tempered Posterior Distributions for Bayesian Inversion Problems. *Mathematics* **2021**, *9*, 784. [CrossRef]

20. Yao, G.; Wu, W.; He, X. High dynamic carrier phase tracking based on adaptive Kalman filtering. In Proceedings of the Chinese Control and Decision Conference (CCDC), Mianyang, China, 23–25 May 2011; pp. 1245–1249.

21. Chen, S.; Gao, Y. Improvement of carrier phase tracking in high dynamic conditions using an adaptive joint vector tracking architecture. *GPS Solut.* **2019**, *23*, 15. [CrossRef]

22. Harsha, S.; Ratnam, V. Implementation of advanced carrier tracking algorithm using adaptive-extended Kalman filter for GNSS receivers. *IEEE Geosci. Remote Sens. Lett.* **2016**, *13*, 1280–1284. [CrossRef]

23. Vila, J.; Closas, P.; Fernández, C.; Lopez, A.; Seco-Granados, G. Adaptive GNSS carrier tracking under ionospheric scintillation: Estimation vs. mitigation. *IEEE Commun. Lett.* **2015**, *19*, 961–964. [CrossRef]

24. Miao, Z.; Lv, Y.; Xu, D.; Shen, F.; Pang, S. Analysis of a variational Bayesian adaptive cubature Kalman filter tracking loop for high dynamic conditions. *GPS Solut.* **2017**, *21*, 111–122. [CrossRef]

25. O'Driscoll, C.; Petovello, G.; Lachapelle, G. Choosing the coherent integration time for Kalman filter-based carri-er-phase tracking of GNSS signals. *GPS Solut.* **2011**, *15*, 345–356. [CrossRef]

26. Yin, Z.; Li, G.; Zhang, Y.; Liu, J. Symmetric-Strong-Tracking-Extended-Kalman-Filter-Based Sensorless Control of Induction Motor Drives for Modeling Error Reduction. *IEEE Trans. Ind. Informat.* **2019**, *15*, 650–662. [CrossRef]

27. Zhou, D.; Xi, Y.; Zhang, Z. A suboptimal multiple fading extended Kalman filter. *Acta Autom. Sin.* **1991**, *17*, 689–695.

28. Gao, W.; Li, J.; Zhou, G.; Li, Q. Adaptive Kalman filtering with recursive noise estimator for integrated SINS/DVL systems. *J. Navig.* **2015**, *68*, 142–161. [CrossRef]

29. Jwo, D.; Chung, F.; Weng, T. *Adaptive Kalman Filter for Navigation Sensor Fusion*; Intech Open: London, UK, 2010; pp. 67–69.

30. Rahimi, M.; Boulet, B. Estimation of the State Variables and Unknown Input of a Two-Speed Electric Vehicle Driveline Using Fading-Memory Kalman Filter. *IEEE Trans. Transp. Electrif.* **2016**, *2*, 210–220. [CrossRef]

31. Soken, H.; Hajiyev, C. Pico satellite attitude estimation via robust unscented Kalman filter in the presence of measurement faults. *ISA Trans.* **2010**, *49*, 249–256. [CrossRef] [PubMed]

32. Jin, D. Adaptive Kalman filtering based on optimal autoregressive predictive model. *GPS Solut.* **2017**, *21*, 307–317. [CrossRef]

33. Ge, Q.; Shao, T.; Wen, C.; Sun, R. Analysis on strong tracking filtering for linear dynamic systems. *Math. Probl. Eng.* **2015**, 648125. [CrossRef]

34. Lo, K.; Lu, Q.; Kwon, W. Comments on 'optimal solution of the two-stage Kalman estimator'. *IEEE Trans. Autom. Control* **2002**, *47*, 198–199.